ACS APPLIED MATERIALS & INTERFACES

Research Article

www.acsami.org

Using a Layer-by-Layer Assembly Method To Fabricate a Uniform and Conductive Nitrogen-Doped Graphene Anode for Indium−Tin Oxide-Free Organic Light-Emitting Diodes

Xinkai Wu,[†] Siying Li,[†] Yanru Zhao,[‡] Yanping Tang,[‡] Jun Liu,[†] Xiaojun Guo,[†] Dongqing Wu,[‡] and Gufeng He*,[†]

[†]National Engineering Lab for TFT-LCD Materials and Technologies, and Department of Electronic Engineering, and [‡]School of Chemistry and Chemical Engineering, Shanghai Jiao Tong University, Shanghai 200240, People's Republic of China

ABSTRACT: Highly conductive, uniform, and transparent nitrogen-doped graphene multilayer films were produced by a layer-by-layer (LbL) assembly method. Such a technique was realized by alternate deposition of graphene oxide modified with the cationic surfactant *N*,*N*,*N*-trimethyl-1-dodecanaminium bromide (CTAB) and the anionic surfactant sodium dodecylbenzenesulfonate. In this way, we can achieve a highly conductive (900 S/cm), uniform, and controllable graphene film in terms of thickness, transmittance, and sheet resistance after high-temperature reduction. The improved conductivity is attributed to better graphitization and nitrogen-doping introduced by CTAB. The organic light-emitting diode using such a multilayer graphene film fabricated by the LbL method as an anode obtains higher current density and luminance at low voltage compared to that with an indium−tin oxide (ITO) anode. Moreover, the current efficiency of graphene-based device is comparable to that of an ITO-based device. It is proved that such a nitrogen-doped multilayer graphene film developed by the LbL assembly technique is a promising candidate for a transparent electrode in organic electronics.

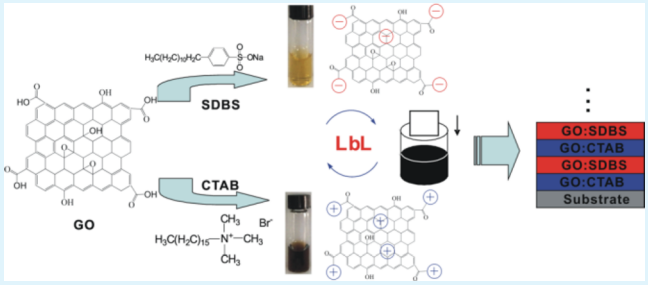

KEYWORDS: *graphene, surfactant, layer-by-layer, nitrogen-doping, OLED*

INTRODUCTION

Recently, flexible organic light-emitting diodes (OLEDs) have drawn considerable research interest due to their unique properties. Among them, high mechanical flexibility is considered as a formidable property compared to that of existing display and lighting technology.[1] Flexible OLEDs require inexpensive, bendable, highly transparent, and conductive electrodes. Up to now, the most widely used transparent electrode material in optoelectronic devices is indium−tin oxide (ITO). However, ITO requires complex fabrication, and the scarcity of indium makes it more and more expensive. Furthermore, it is fragile upon stretch and bending, which limits its application when flexibility is required.[2] Graphene is a two-dimensional pure carbon sheet, showing unique electrical, optical, and mechanical properties.[3,4] With these special merits, graphene has recently attracted enormous interest in the application of organic light emitting diodes (OLEDs),[5] solar cells,[6] field-effect transistors,[7] sensors,[8] and flexible displays,[9] and it is considered as one of the candidates with the most potential to replace ITO.

However, complicated processing and the insolubility of graphene in solution render it challenging to obtain highly conductive and uniform large-area graphene films. One of the most promising methods to prepare large-area graphene electrode film is to reduce solution-processed graphene oxide (GO) with different treatments. To produce graphene on a large quantity, natural graphite is often oxidized to form GO, which is considered as a fantastic precursor.[10] However, defects and oxygen functional groups are inevitably introduced into the carbon network sheet during oxidation, leading to an insulating property for GO films. Reduced graphene oxide (rGO) with high conductivity can be obtained by traditional thermal annealing at high temperature and chemical reduction at low temperature of GO films to remove oxygen groups. However, the residual defects on the graphene basal plane and the quick reaggregation of graphene sheets into graphite limit the conductivity and superficial quality of rGO film.[11,12] Therefore, healing the defects on the graphene plane and improving the dispersion of graphene sheets in solution are necessary to obtain a highly conductive and smooth graphene film.

Graphene films can be fabricated by many methods, such as layer-by-layer (LbL) assembly,[13] spin-coating,[14] rod-coating,[15] spray-coating,[16] and chemical vapor deposition (CVD).[17] Among these various methods, the LbL assembly technique using different film fabrication processes and materials can yield multilayer graphene thin films with highly superficial quality and

Received: April 30, 2014
Accepted: August 27, 2014
Published: August 27, 2014

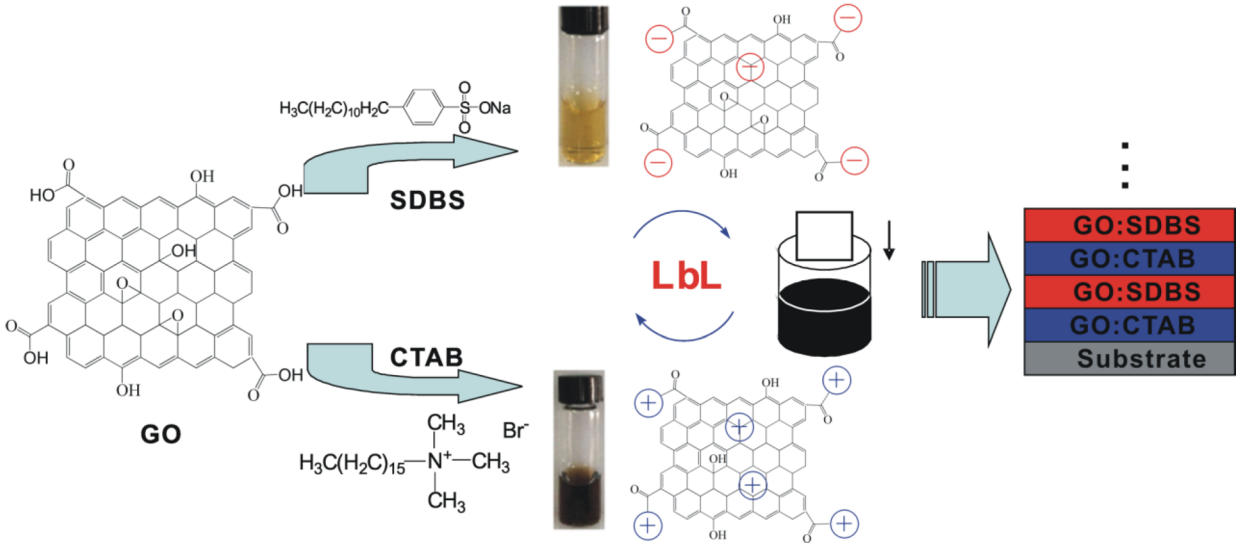

Figure 1. Schematic diagram of LbL assembly of GO:CTAB and GO:SDBS.

controlled structure.[18] This process delivers high throughput, low cost, and simple fabrication and, hence, is considered as one of the most auspicious methods to prepare large-area graphene films. Lee et al.[19] reported using LbL assembly of positively and negatively charged rGO sheets to develop multilayer thin films, and the lowest sheet resistance is 2500 Ω per square at 75% transmittance after 1000 °C thermal annealing in H_2 atmosphere. Tang et al.[20] reported that the cationic surfactant cetyltrimethylammonium bromide (C_{16}TAB) and the anionic surfactant sodium dodecyl sulfate (SDS) as positive and negative agents could interact with graphene to produce rGO multilayer thin films by LbL assembly. The obtained rGO multilayer films had conductivity varying from 80 to 110 S/cm. Park et al.[21] show a simple method to fabricate graphene multilayer films by LbL assembly of carboxylic acid-functionalized graphene and amine-functionalized graphene based on electrostatic interactions. After 900 °C thermal annealing, the graphene film with 42 bilayers can obtain the lowest sheet resistance of about 700 Ω per square with a transmittance of 72%, but the root-mean-square (rms) roughness of the graphene film is still about 5.6 nm. These graphene films, with not high enough conductivity and uniformity, are unsuitable to be used in OLEDs.

In this paper, a highly conductive, smooth, and transparent graphene film is produced by the LbL assembly method. Specifically, we have used the cationic surfactant *N,N,N*-trimethyl-1-dodecanaminium bromide (CTAB) and the anionic surfactant sodium dodecylbenzenesulfonate (SDBS) as positive and negative agents interacting with GO. These surfactants can improve the dispersion of GO in solution, and high-quality GO films can be fabricated by LbL assembly. The thickness, transmittance, and sheet resistance of the film can be controlled by varying the deposition cycles. Meanwhile, we have found that, after 1000 °C thermal annealing, the conductivity of graphene thin film can be increased to about 900 S/cm due to better graphitization and nitrogen-doping on the graphene plane to heal the defects. The nitrogen atom is introduced by thermal decomposition of the cationic surfactant CTAB on the graphene basal plane. The device with multilayer graphene as the anode can obtain higher current density and luminance compared with those of an ITO anode, and its current efficiency can reach 4.5 cd/A, which is comparable to that of the device with an ITO anode.

EXPERIMENTAL SECTION

Preparation of Negatively and Positively Charged Oxide Graphene Solution. All the chemicals were purchased from Sigma-Aldrich and were analytical reagent grade without further purification. Graphene oxide was prepared from graphite powder using a modified Hummers method.[22−24] Positively charged GO was synthesized by combining the cationic surfactant CTAB and pristine GO at a weight ratio of 10:1 in *N,N*-dimethylformamide (DMF) solvent. Similarly, negative charged GO was obtained by blending SBDS and GO at a weight ratio of 10:1 in deionized (DI) water. Both GO:CTAB and GO:SBDS solutions were ultrasonicated for 1 h and then stirred for 24 h. Finally, dark brown and golden yellow colored solutions are obtained for GO:CTAB and GO:SBDS solution, respectively, and each of them contains 0.3 mg/mL concentration of GO.

LbL Assembly of Charged Graphene Nanosheets. Quartz substrate was cleaned with sonication in DI water, acetone, and 2-propanol, respectively, and then treated with oxygen plasma at 20 W power for 2 min to produce a negatively charged surface.[16] After that, the substrate was baked at a temperature of 100 °C for 10 min to remove the residual solvents. The treated substrate was slowly dipped into positively charged GO:CTAB solution at a speed of 18 mm/min. After being fully immersed into solution and kept for 20 s, the substrate was pulled up at a speed of 6 mm/min followed by rinsing with DMF. The substrate with GO:CTAB film was dried on the hot plate at 150 °C for 15 min. On top of the GO:CTAB film, the GO:SDBS film was fabricated using a similar dip-coating process, with a rinsing step with DI water. The deposition of one GO:CTAB and one GO:SDBS layer is defined as one deposition cycle. We can get the desired multilayer film with a certain number of deposition cycles. The whole fabrication process is shown in Figure 1. However, after finishing the whole dipping deposition, the GO film at the back side of the substrate was completely removed with ethanol. Finally, the assembled multilayer film was treated in a furnace at 1000 °C for 2 h for reduction to obtain rGO multilayer film.

OLED Devices. A thin layer of PEDOT:PSS (AI4083), purchased from H. C. Starck, was spin-coated on the rGO film as hole-injecting layer (HIL), and then the substrate was transferred into a high-vacuum system at a base pressure of 10^{-6} Torr for the following deposition of organic and metal layers to finish the OLED fabrication. The OLED devices used 60 nm of *N,N′*-bis(naphthalen-1-yl)-*N,N′*-bis(phenyl)-benzidine (NPB) as the hole-transporting layer (HTL), 50 nm of tris-8-hydroxyquinoline aluminum (Alq_3) as both electron-transporting layer (ETL) and emitting layer (EML), 1 nm of 8-hydroxyquinolinato lithium (Liq) as electron-injecting layer (EIL), and 100 nm of aluminum (Al) as cathode. The thickness of the organic layer was monitored in situ by a calibrated quartz-crystal monitor in the vacuum deposition chamber. The active area defined by the overlap of the anode and the Al cathode

was around 3 × 3 mm^2. The deposition rate was monitored in situ by a quartz-crystal monitor. Figure 2 shows the schematic cross section of the fabricated device stack.

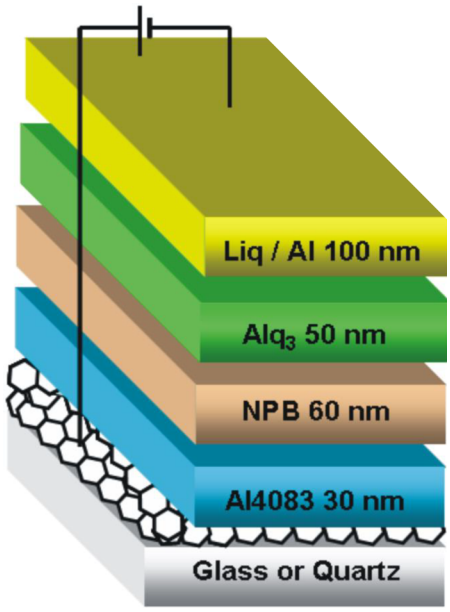

Figure 2. Schematic cross section of the OLED device.

Characterization. The thickness of the obtained graphene film was measured by using a KLA-Tencor AlphaStep D-120 Stylus Profiler. The transmittance of the rGO films were characterized by MAPADA UV-3100PC spectrophotometer. The chemical bonding and elemental compositions of the films were analyzed by Fourier transform infrared (FTIR) spectroscopy (Nicolet 6700) and X-ray photoelectron spectroscopy (XPS) (AXIS Ultra). The roughness and surface morphology were analyzed by an atomic force microscope (AFM) (Bioscope SPM). The conductivity of the film was evaluated from sheet-resistance measurements by means of a four-point probe system. OLED device performances were characterized by computer-controlled Keithley 2400 source meter and Topcon BM-7A luminance colorimeter.

RESULTS AND DISCUSSION

Figure 3 illustrates the Fourier transform infrared spectroscopy (FTIR) spectra of GO, GO:SDBS, and GO:CTAB, respectively. As shown in Figure 3a, the broad peak at 3406 cm^{-1} is from −OH groups, and the other broad peak at 1127 cm^{-1} is attributed to C−O−C bonds on GO sheets. Two narrow peaks assigned to the carbonyl group (C═O stretching) and the skeletal vibration of graphitic domains on GO sheets can be observed at 1740 and

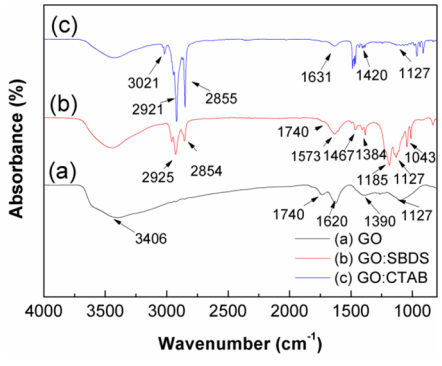

Figure 3. FTIR spectra of GO (a), GO:SDBS (b), and GO:CTAB (c).

1620 cm^{-1}. For GO:SDBS (Figure 3b), the C−H groups for SDBS are shown by the peaks at 2925 and 2854 cm^{-1}, and phenyl groups for SDBS are indicated by the strong peak at 1573 cm^{-1}.[25] The peak at 1467 cm^{-1} is attributed to a C−H bending vibration, and two obvious peaks at 1185 and 1043 cm^{-1} are ascribed to the antisymmetric and symmetric stretching vibrations of S═O on SDBS. On the other hand, the peak at 1127 cm^{-1} attributed to the C−O−C bonds of GO can also be observed, and the peak at 1390 cm^{-1} assigned to carbonyl groups on GO is shifted to 1384 cm^{-1} due to the influence of SDBS by electrostatic force. This result confirms that SDBS has grafted into GO layers. The peaks at 3021, 2921, and 2855 cm^{-1} in Figure 3c correspond to N−H and $-CH_2$ stretching vibrations in CTAB. The peak at 1127 cm^{-1} can also be observed when mixed with CTAB, as shown in Figure 3c, but the intensity is much weaker because the weight ratio of pristine GO and CTAB is only 1:10. Meanwhile, the peak shown at 1420 cm^{-1} is ascribed to the symmetric vibration of the acid amides group, which is caused by the combination of carbonyl and amino groups on GO and CTAB by Coulombic force. The original $C_{19}H_{42}N^+$ asymmetric bending peak for CTAB shifts from 1611 to 1631 cm^{-1}, which is caused by the overlap with the peak of graphitic domain vibration.[26]

In order to confirm that SDBS and CTAB have grafted on GO layers, thermogravimetric analysis (TGA) was conducted to study the thermal stability of GO, GO:CTAB, and GO:SDBS. The samples are heated to 700 °C at a rate of 10 °C/min within a nitrogen atmosphere. As shown in Figure 4, the overall weight

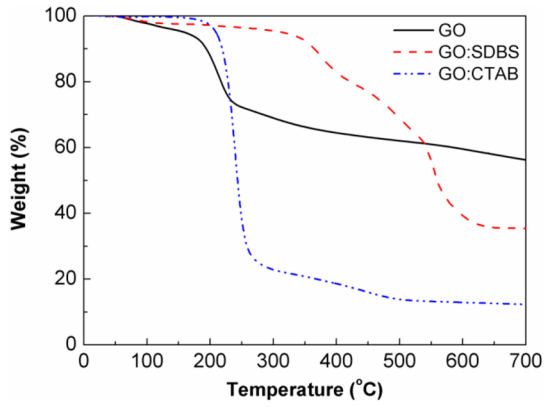

Figure 4. Thermogravimetric analysis of GO, GO:SDBS, and GO:CTAB.

loss of GO is about 46% around 200 °C.[25] It is mainly attributed to the removal of labile oxygen functional groups on GO sheets.[27] As for GO:SDBS, about 68% weight fraction loss is observed from 350 to 650 °C, which may be caused by the decomposition of SDBS (combined with layered GO via weaker $\pi-\pi$ and hydrophobic interactions) and some oxygen functional groups on GO sheets.[28] The curve of GO:CTAB shows a fast weight reduction at around 200 °C, and it may be caused by the decomposition of CTAB and labile oxygen functional groups on GO; 85% overall weight loss is observed for GO:CTAB. The increase of weight loss is attributed to the combining of CTAB and GO sheets through strong electrostatic ionic interactions.[29]

Figure 5 shows the sheet resistance, thickness, and transmittance of rGO films after annealing with different deposition cycles in the LbL assembly process. As shown in Figure 5a, the sheet resistance decreases dramatically with the increase of cycles. The too high sheet resistance of rGO multilayers films with less than seven cycles is mainly attributed to the poor

dx.doi.org/10.1021/am502629b | ACS Appl. Mater. Interfaces 2014, 6, 15753−15759

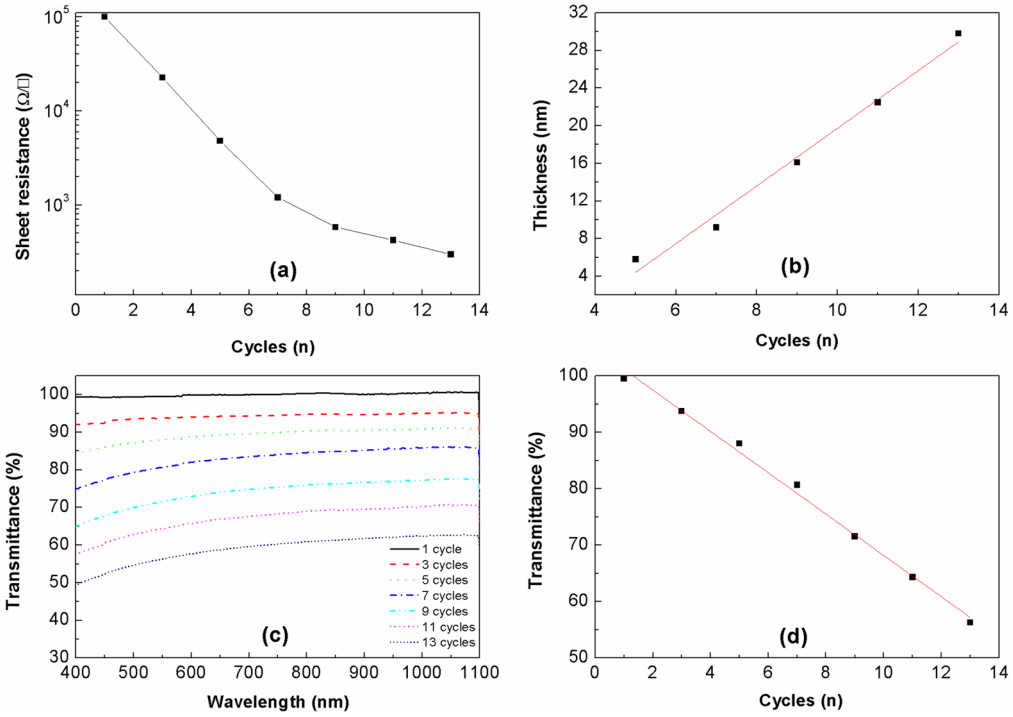

Figure 5. Sheet resistance (a), thickness (b), transmittance (c), and transmittance measured at 550 nm (d) of the rGO multilayers films as a function of the number of cycles after annealing.

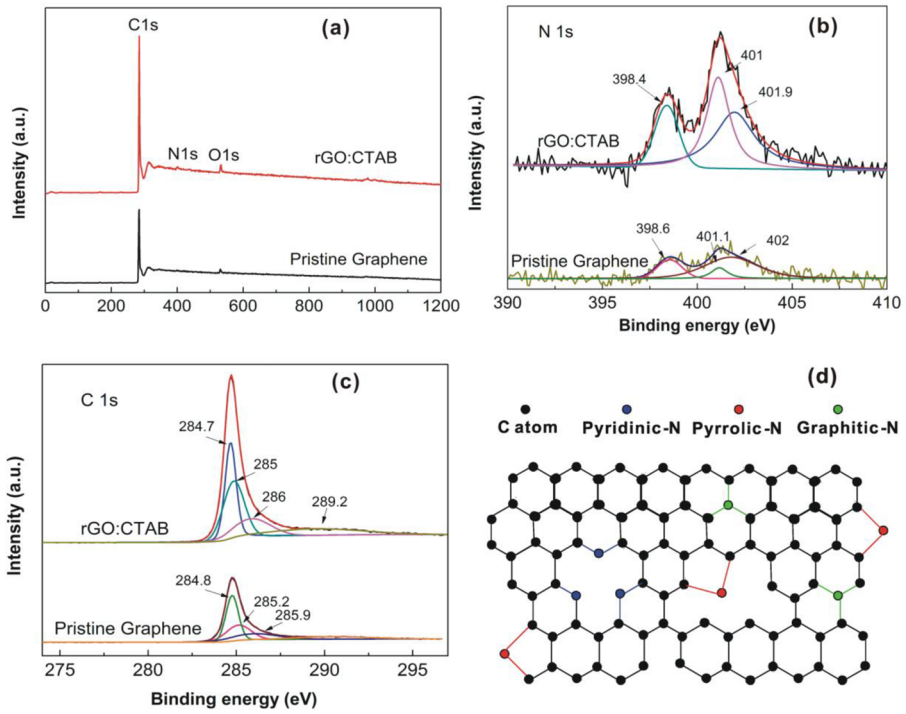

Figure 6. (a) XPS spectra of rGO:CTAB and pristine graphene after thermal annealing at 1000 °C in a nitrogen atmosphere. N 1s peaks (b) and C 1s peaks (c) of rGO:CTAB and pristine graphene. (d) Schematic structure of nitrogen-doped rGO:CTAB.

connection of rGO sheets, and the sheet resistance of films of rGO multilayers beyond seven deposition cycles decreases linearly. Opposite to the sheet resistance, the thickness of rGO multilayer films linearly increases with an increasing number of cycles (Figure 5b). Figure 5c shows the transmittance of rGO multilayers films with a different number of cycles. The transmittance measured at 550 nm also decreases linearly with an increasing number of cycles (in Figure 5d). Therefore, the sheet resistance, thickness, and transmittance of rGO films can be precisely controlled via such a LbL assembly technique. In this paper, the rGO multilayers film with 13 deposition cycles after thermal annealing at 1000 °C has the lowest sheet resistance (298 Ω per square), with about 60% transmittance at 550 nm. The conductivity is calculated to be about 900 S/cm. The higher

dx.doi.org/10.1021/am502629b | ACS Appl. Mater. Interfaces 2014, 6, 15753−15759

conductivity is mainly caused by better graphitization and nitrogen-doping on the graphene plane to heal the defects. Thermal decomposition of the cationic surfactant CTAB on the graphene basal plane can provide such nitrogen atoms.[30,31] The results can be further confirmed by X-ray photoelectron spectroscopy (XPS).

As shown in Figure 6a, three peaks at 284.2, 399.7, and 532.7 eV attributed to C 1s, N 1s, and O 1s of the rGO:CTAB sample are shown in the XPS scan spectrum. However, the peak of N 1s at 399.7 eV is hardly detected in the pristine graphene. The atomic percentage of doped nitrogen for rGO:CTAB sample is calculated to be about 2.2% in Figure 6a, which is larger than the percentage in pristine graphene sample (only 1.5%). The GO:CTAB and pristine GO powders are both thermally annealed at 1000 °C in nitrogen atmosphere. Therefore, the nitrogen atoms are mainly provided by the thermal decomposition of the cationic surfactant CTAB on the graphene basal plane and the annealing environment of the nitrogen atmosphere. As shown in Figure 6b, the N 1s peak has three components centered at 398.4, 401, and 401.9 eV, corresponding to pyridinic-N, pyrrolic-N, and graphitic-N, respectively. Pyridinic-N stands for one N atom bonding with two carbon atoms at the edges of graphene sheets, and each N atom can devote one p-electron to the aromatic π system. Pyrrolic-N indicates that one N atom can bond with two carbon atoms in five-membered heterocyclic rings, and each N atom provides two p-electrons to the aromatic π system. These two structures indicate the healing defects at the edges of graphene lattice and formation of a p−π conjugated system, which can improve the conductivity of the graphene.[32] Graphitic-N atom can insert into the graphene sheet and replace one carbon atom on the graphene crystal. Therefore, each N atom is bonded with three carbon atoms to form a stable structure, which may reduce the aromatic π system of the graphene sheet and decrease the charge transport pathways on the graphene plane.

The relative atomic ratios of three types of doped N atoms for pristine graphene and rGO:CTAB samples are shown in Table 1.

Table 1. Detailed Peak Types and Relative Atomic Ratios (%) of N 1s Spectra from rGO:CTAB and Primitive Graphene Samples after Annealing from XPS Analysis

	pyridinic-N	pyrrolic-N	graphitic-N
rGO:CTAB	0.954	0.659	0.587
pristine graphene	0.317	0.549	0.634

It is worthwhile to note that the pyridinic-N and pyrrolic-N contents in rGO:CTAB sample are higher than those in pristine graphene, but the graphitic-N content clearly decreases. It means that the addition of CTAB can improve the atomic percentage of doped nitrogen and that more N atoms will heal defects at the edges of the graphene lattice to form a p−π conjugated system, which can improve the conductivity of the rGO:CTAB. As shown in the C 1s spectrum (Figure 6c), a comparison of the atomic percentage for doped nitrogen in primitive graphene and rGO:CTAB samples can also be conducted. The peak at 284.6 eV ascribed to the graphite-like sp^2 C indicates that the most C atoms are arranged like a conjugated honeycomb lattice. The C−N bonds can also be reflected with peaks centered at 285.7 and 286.6 eV, which are attributed to the N sp^2 C and N sp^3 C, respectively. The C−O type bond is mainly shown by the peak at 288.9 eV.[33,34] As shown in Figure 6c, the contents of the C−N bonds in rGO:CTAB sample are larger than that in pristine graphene sample, indicating that more N atoms have been doped into the rGO:CTAB plane.

The surface morphology of rGO films after annealing was observed by atomic force microscopy (AFM). As shown in Figure 7a, separated rGO sheets can be obviously observed on the obtained film with one cycle, and the dimensions of the graphene sheets are from several hundred nanometers to several micrometers. In Figure 7b, an incomplete film of rGO can be observed clearly. Some dark and bright areas are shown in the image, which means that the rGO film is not uniform, resulting in high surface rms roughness (2.15 nm) and high sheet resistance. In Figure 7c, the individual sheets seem to merge together, but some wrinkles can also be observed, and the surface rms roughness decreases to about 1.99 nm. With the deposition cycles increasing to 9 and 11 (Figure 7d,e), the surface morphology becomes more uniform, and the clear boundary of the overlapped graphene sheets is hard to observe.[16] The surface rms roughness decreases down to about 1.96 and 1.35 nm. However, some wrinkles are observed on the rGO film surface with 13 cycles, as shown in Figure 7f, and the surface rms roughness of the obtained rGO multilayer film is increased to about 1.83 nm. It means that the film with more deposition cycles can lower its sheet resistance, but the surface rms roughness will increase. The rGO sheets may be rearranged to form a more compact graphene film after annealing, so the surface morphology and rms roughness are changed during high-temperature treatment.[19]

Considering both the conductivity and uniformity, we fabricated an OLED device using a rGO film with 11 cycles as anode to compare it with an OLED using a conventional ITO anode. Parts a and b of Figure 8 show the current density−voltage and luminescence−voltage characteristics of OLEDs based on rGO film and ITO anodes, respectively. The turn-on voltage is 2.8 and 4.5 V for OLEDs with rGO and ITO anodes. At a voltage of 8 V, the luminance of the device with the ITO anode is 106 cd/m^2, while that of the device with the rGO anode is 120 cd/m^2. Moreover, the current density of OLEDs with the rGO anode is higher at low voltage than the device with the ITO anode. The energy diagram of full OLED devices can be observed in Figure 8d. The work function of ITO (4.3 eV) is much lower than the highest occupied molecular orbital (HOMO) level of NPB, and the large barrier makes it difficult to inject holes from the anode into the NPB. Hence, the turn-on voltage is larger, whereas the luminance is smaller with the ITO anode. The higher work function of nitrogen-doped graphene anode improves the hole injection into the hole transport layer at low voltage, and higher luminance and current density are obtained. As shown in Figure 8c, the slightly decreased current efficiency of the device with the rGO anode is attributed to less balanced electron−hole recombination due to excess hole injection from the rGO anode. However, the current efficiency of the OLEDs with the rGO anode is still about 4.5 cd/A. The optical image of green OLEDs with rGO hybrid films is shown as an inset.

CONCLUSIONS

In conclusion, we successfully fabricated highly conductive, uniform, and transparent graphene films by the LbL assembly method. The cationic surfactant CTAB and the anionic surfactant SDBS were used as positive and negative agents interacting with graphene. The sheet resistance, thickness, and transmittance of the film can be controlled by adjusting the deposition cycles. The rGO multilayers film with 13 cycles after thermal annealing at 1000 °C has the lowest sheet resistance of

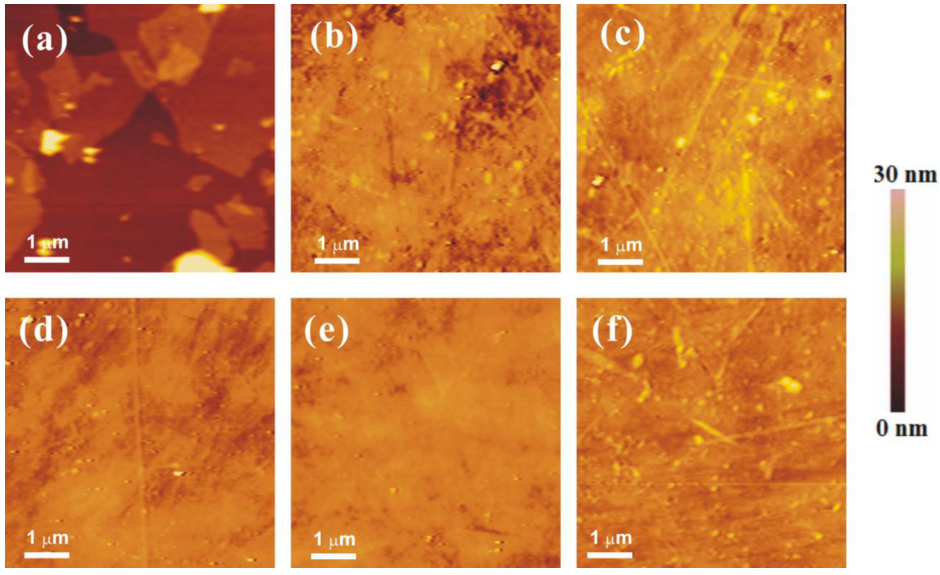

Figure 7. AFM images of rGO multilayers with (a) 1, (b) 5, (c) 7, (d) 9, (e) 11, and (f) 13 cycles on quartz substrates after 1000 °C annealing.

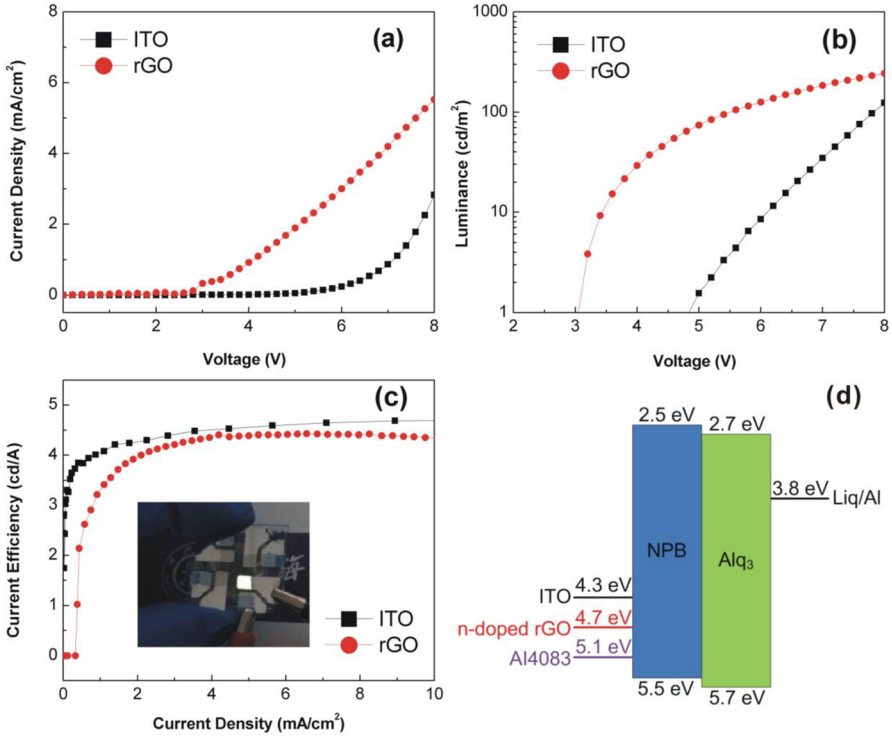

Figure 8. (a) Current density−voltage, (b) luminance−voltage, (c) current efficiency−current density characteristics, and (d) the energy diagram of full OLED devices with ITO and rGO films with 11 cycles as anodes.

298 Ω per square with about 60% transmittance at 550 nm. The nitrogen atoms in the cationic surfactant CTAB help heal the defects during the reduction at high temperature. Considering the conductivity and uniformity of the thin films, we fabricated an OLED using rGO film with 11 cycles as anode. The OLED device can reach a luminance and current efficiency of about 120 cd/m^2 and 4.5 cd/A at 8 V, and these values are comparable to those of the device with an ITO anode.

AUTHOR INFORMATION

Corresponding Author

*E-mail: gufenghe@sjtu.edu.cn. Tel.: +86-21-34207045. Fax: +86-21-34204371.

Author Contributions

The manuscript was written through contributions of all authors. All authors have given approval to the final version of the manuscript.

Notes

The authors declare no competing financial interest.

■ ACKNOWLEDGMENTS

The present work was supported by 973 Program (2013CB328803, 2013CB328804), the National Natural Science Foundation of China (61377030), and the Science and Technology Commission of Shanghai Municipal (12JC1404900).

■ REFERENCES

(1) Peng, L. W.; Feng, Y. Y.; Feng, W. Transparent, Conductive, and Flexible Multiwalled Carbon Nanotube/Graphene Hybrid Electrodes with Two Three-Dimensional Microstructures. *J. Phys. Chem. C* **2012**, *116*, 4970−4978.

(2) Huang, Y. L.; Baji, A.; Tien, H. W.; Yang, Y. K.; Yang, S. Y. Self-Assembly of Silver−Graphene Hybrid on Electrospun Polyurethane Nanofibers as Flexible Transparent Conductive Thin Films. *Carbon* **2012**, *10*, 3473−3481.

(3) Lahiri, I.; Verma, V. P.; Choi, W. B. An All-Graphene Based Transparent and Flexible Field Emission Device. Carbon. *Carbon* **2011**, *49*, 1614−1619.

(4) Wöbkenberg, P. H.; Eda, G.; Leem, D. S.; Mello, J. C. d. Reduced Graphene Oxide Electrodes for Large Area Organic Electronics. *Adv. Mater.* **2011**, *23*, 1558−1562.

(5) Han, T. H.; Lee, Y. B.; Choi, M. R.; Woo, S. H.; Bae, S. H.; Hong, B. H.; Ahn, J. H.; Lee, T. W. Extremely Efficient Flexible Organic Light-Emitting Diodes with Modified Graphene Anode. *Nat. Photonics* **2012**, *6*, 105−110.

(6) Miao, X. C.; Tongay, S.; Petterson, M. K.; Berke, K. High Efficiency Graphene Solar Cells by Chemical Doping. *Nano Lett.* **2012**, *12*, 2745−2750.

(7) Reddy, D.; Register, L. F.; Carpenter, G. D.; Banerjee, S. K. Graphene Field-Effect Transistors. *J. Phys. D: Appl. Phys.* **2012**, *45*, 019501.

(8) Nagelli, E.; Naik, R.; Xue, Y. H.; Gao, Y. X.; Zhan, M.; Dai, L. M. Sensor Arrays from Multicomponent Micropatterned Nanoparticles and Graphene. *Nanotechnology* **2013**, *24*, 444010.

(9) Zhang, C. H.; Fu, L.; Liu, N.; Liu, M. H.; Wang, Y. Y.; Liu, Z. F. Synthesis of Nitrogen-Doped Graphene Using Embedded Carbon and Nitrogen Sources. *Adv. Mater.* **2011**, *23*, 1020−1024.

(10) Liao, W. H.; Yang, S. Y.; Wang, J. Y. Effect of Molecular Chain Length on the Mechanical and Thermal Properties of Amine-Functionalized Graphene Oxide/Polyimide Composite Films Prepared by in Situ Polymerization. *ACS Appl. Mater. Interfaces* **2013**, *5*, 869−877.

(11) Singh, A. K.; Ahmad, M.; Singh, V. K. Tailoring the Electrical Properties of Graphene Layers by Molecular Doping. *ACS Appl. Mater. Interfaces* **2013**, *5*, 5276−5281.

(12) Shi, S. W.; Sadhu, V.; Moubah, R.; Schmerber, G.; Bao, Q. Y.; Ravi, S.; Silva, P. Solution-Processable Graphene Oxide as an Efficient Hole Injection Layer For High Luminance Organic Light-Emitting Diodes. *J. Mater. Chem. C* **2013**, *1*, 1708−1712.

(13) Pei, S.; Zhao, J.; Du, J.; Ren, W.; Cheng, H. M. Direct Reduction of Graphene Oxide Films into Highly Conductive and Flexible Graphene Films by Hydrohalic Acids. *Carbon* **2010**, *48*, 4466−4474.

(14) Shin, H. J.; Kim, K. K.; Benayad, A.; Yoon, S. M.; Park, H. K.; Jung, I. S.; Jeong, H. K.; Kim, J. M.; Choi, J. Y.; Lee, Y. H. Efficient Reduction of Graphite Oxide by Sodium Borohydride and Its Effect on Electrical Conductance. *Adv. Funct. Mater.* **2009**, *19*, 1987−1992.

(15) Wang, J.; Liang, M. H.; Fang, Y.; Qiu, T. F.; Zhang, J.; Zhi, L. J. Rod Coating: Towards Large-Area Fabrication of Uniform Reduced Graphene Oxide Films for Flexible Touch Screens. *Adv. Mater.* **2012**, *24*, 2874−2878.

(16) Becerril, H. A.; Mao, J.; Liu, Z.; Stoltenberg, R. M.; Bao, Z. N.; Chen, Y. Evaluation of Solution-Processed Reduced Graphene Oxide Films as Transparent Conductors. *ACS Nano* **2008**, *2*, 463−470.

(17) Kim, K. S.; Zhao, Y.; Jang, H.; Lee, S. Y.; Kim, J. M.; Kim, K. S.; Ahn, J. H.; Kim, P.; Choi, J. Y.; Hong, B. H. Large-Scale Pattern Growth of Graphene Films for Stretchable Transparent Electrodes. *Nature* **2009**, *457*, 706−710.

(18) Shen, J. F.; Hu, Y. Z.; Li, C.; Qin, C.; Shi, M.; Ye, M. X. Layer-by-Layer Self-Assembly of Graphene Nanoplatelets. *Langmuir* **2009**, *25*, 6122−6128.

(19) Lee, D. W.; Hong, T. K.; Kang, D. W.; Lee, J.; Heo, M.; Kim, J. Y.; Kim, B. S.; Shin, H. S. Highly Controllable Transparent and Conducting Thin Films Using Layer-by-layer Assembly of Oppositely Charged Reduced Graphene Oxides. *J. Mater. Chem.* **2011**, *21*, 3438−3442.

(20) Tang, Q. W.; Tang, Z. Y.; Wu, J. H.; Lin, J. M.; Oh, I. Highly Conducting Multilayer Films from Graphene Nanosheets by a Spin Self-Assembly Method. *J. Mater. Chem.* **2011**, *21*, 5378−5385.

(21) Park, J. S.; Cho, S. M.; Kim, W. J.; Park, J. Y.; Yoo, P. J. Fabrication of Graphene Thin Films Based on Layer-by-Layer Self-Assembly of Functionalized Graphene Nanosheets. *ACS Appl. Mater. Interfaces* **2011**, *3*, 360−368.

(22) Zeng, G. h.; Xing, Y. B.; Gao, J.; Wang, Z. Q.; Zhang, X. Unconventional Layer-by-Layer Assembly of Graphene Multilayer Films for Enzyme-Based Glucose and Maltose Biosensing. *Langmuir* **2010**, *26*, 15022−15026.

(23) Matyba, P.; Yamaguchi, H.; Eda, G.; Chhowalla, M.; Edman, L.; Robinson, N. D. Graphene and Mobile Ions: The Key to All-Plastic, Solution-Processed Light-Emitting Devices. *ACS Nano* **2010**, *4*, 637−642.

(24) Wang, Y.; Tong, S. W.; Xu, X. F.; Özyilmaz, B.; Loh, K. P. Interface Engineering of Layer-by-Layer Stacked Graphene Anodes for High-Performance Organic Solar Cells. *Adv. Mater.* **2011**, *23*, 1514−1518.

(25) Wu, X. K.; Liu, J.; Wu, D. Q.; Zhao, Y. R.; Shi, X. D.; Wang, J.; Huang, S. J.; He, G. F. Highly Conductive and Uniform Graphene Oxide Modified PEDOT:PSS Electrodes for ITO-Free Organic Light Emitting Diodes. *J. Mater. Chem. C* **2014**, *2*, 4044−4050.

(26) Song, C. P.; Wu, D. Q.; Zhang, F.; Liu, P.; Lu, Q. H.; Feng, X. L. Gemini Surfactant Assisted Synthesis of Two-Dimensional Metal Nanoparticles/Graphene Composites. *Chem. Commun.* **2012**, *48*, 2119−2121.

(27) Rodil, S. V.; Paredes, J. I.; Alonso, A. M. Preparation of Graphene Dispersions and Graphene−Polymer Composites in Organic Media. *J. Mater. Chem.* **2009**, *19*, 3591−3593.

(28) Kim, L.; Trang, H. Y.; Tung, T. T.; Kim, T. Y.; Yang, W. S.; Kim, H.; Suh, K. S. Preparation and Characterization of Graphene Composites with Conducting Polymers. *Polym. Int.* **2012**, *61*, 93−98.

(29) Zhang, K.; Mao, L.; Zhang, L. L.; Chan, H. S.; Zhao, X. S.; Wu, J. H. Surfactant-Intercalated, Chemically Reduced Graphene Oxide for High Performance Supercapacitor Electrodes. *J. Mater. Chem.* **2011**, *21*, 7302−7307.

(30) Bonaccorso, F.; Sun, Z.; Hasan, T.; Ferrari, A. C. Graphene Photonics and Optoelectronics. *Nat. Photonics* **2010**, *4*, 611−622.

(31) Chang, H. X.; Wang, G. F.; Yang, A.; Tao, X. M.; Liu, X. Q.; Shen, Y. D.; Zheng, Z. J. A Transparent, Flexible, Low-Temperature, and Solution-Processible Graphene Composite Electrode. *Adv. Funct. Mater.* **2010**, *20*, 2893−2902.

(32) Gao, H.; Song, L.; Guo, W. H.; Huang, L.; Yang, D. Z.; Wang, F. C.; Zuo, Y. L.; Fan, X. L.; Liu, Z.; Gao, W.; Vajtai, R.; Hackenberg, K.; Ajayan, P. M. A Simple Method To Synthesize Continuous Large Area Nitrogen-Doped Graphene. *Carbon* **2012**, *50*, 4476−4482.

(33) Wang, G. Q.; Xing, W.; Zhuo, S. P. Nitrogen-Doped Graphene as Low-Cost Counter Electrode for High-Efficiency Dye-Sensitized Solar Cells. *Electrochim. Acta* **2013**, *92*, 269−275.

(34) Lai, L. F.; Potts, J. R.; Zhan, D.; Wang, L.; Poh, C. K.; Tang, C. H.; Gong, H.; Shen, Z. X.; Lin, J. Y.; Ruoff, R. S. Exploration of the Active Center Structure of Nitrogen-Doped Graphene-Based Catalysts for Oxygen Reduction Reaction. *Energy Environ. Sci.* **2012**, *5*, 7936−7942.